การประชุมวิชาการเครือข่ายวิศวกรรมเครื่องกลแห่งประเทศไทยครั้งที่ 18
18-20 ตุลาคม 2547 จังหวัดขอนแก่น

Local Grid Refinement by Residual Error Estimation for Heat Conduction Simulation with Finite Volume Method

Withaya WATTANANUKULCHAI and Kuntinee MANEERATANA*
Department of Mechanical Engineering, Faculty of Engineering, Chulalongkorn University,
Phaya Thai Road, Pathum Wan, Bangkok 10330 Thailand
Tel: 0-2218-6610, Fax: 0-2252-2889, E-mail: doodede@yahoo.com, kuntinee.m@chula.ac.th

Abstract

This paper presents the utilisation of local grid refinement (LGR) in conjunction with a residual error estimator for 2D heat conduction problems to obtain grid independent solutions with unstructured finite volume method (FVM). LGR increases the accuracy and reduces computational costs by refining only parts of the computational domain where small control volumes are needed in the *h*-refinement manner. First, the initial solutions are obtained with coarse grids. Then, the simplified residual error estimator, calculated from the discrepancy between the volume integration and face interpolation, is used to identify cells for refinement in the next level. The procedure is repeated until residuals of all control volumes do not exceed the prescribed factorisation of the mean residual. A 2D heat conduction problem is used as the test case. The initial grid, consisting of 32 control volumes, are refined to the final mesh with 134 cells in 3 refinement levels. In all, the residual indicator is reduced from 1.73°C to 0.80°C while the normalised mean error and its standard deviation fall from 0.487°C to 0.173°C and 3.50° to 1.41°C, respectively.

Keywords Local grid refinement, residual error estimation, finite volume method.

1. Introduction

Over the years, a large number of adaptive grid methods have been proposed to ensure the grid independent solutions of partial differential equations (PDEs). They can be categorised into 3 main strategies, namely the *h*-, *r*- and *p*-refinements (Figure 1). The *h*-refinement uses the static re-gridding approach such that new nodes are added when they are required or removed when they are not. In *r*-refinement or dynamic regridding, nodes are moved continuously in the space – time domain and the discretisation of PDEs is coupled with motion of the grid. The third approach, *p*-refinement, increases the order of spatial approximation, usually by employing higher order of elements.

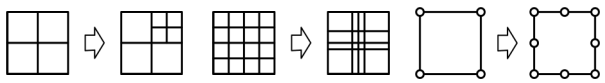

a) *h*-refinement b) *r*-refinement c) *p*-refinement

Figure 1 Concepts of main refinement strategies

Of these approaches, the *h*-refinement is the most straightforward as grids are refined and computational points are added in required regions. It is also popular with structured grids in which the refined control volumes are considered as additional layers over the main grids such that the structured discretisation is superficially retained [1].

The concept of *h*-refinement is not only used to adapt meshes for grid independent solutions but also for the multi-grid acceleration [2], [3] which speeds up the solution convergence rate by solving governing equations with successive cycles of refined and coarsen meshes of the whole domain as the high frequency residuals are eliminated in coarse grids and the low frequency errors are not dominant to fine meshes.

The algorithm inevitably involves assuming an initial grid and the calculation of the solution set of this grid by any numerical simulations, such as finite element or finite volume methods. The grid independency of the results is then determined; if the grid independent condition is not obtained, the problematic regions are refined and repeatedly solved as shown in Figure 2.

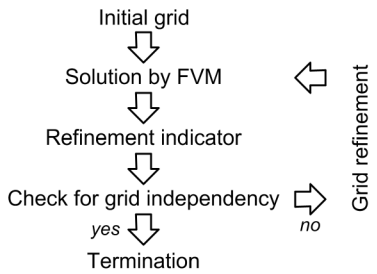

Figure 2 Local grid refinement algorithm

An important procedure in LGR is the identification of cells that should be refined. First, the appropriate variables must be identified. Mostly, the dependent variables, such as temperature in energy equations, displacement in solid momentum equations or pressure and velocity in fluid flows, are used. Occasionally, derived quantities, such as curvature [4], provide a better choice.

From these control variables, the error indicators are specified and compared with the prescribed refinement criterion to mark the problematic regions out. Mostly, the values of double gradient of variables are used as the errors approach zero with linear distribution of variables [5]. As before, some other

relationships may be identified for specific cases such as the adaptive function that are functions both velocity and pressure [6].

There are many approaches of grid refinements for different shapes of control volumes. For initial rectangular grids, the simplest and most common technique is the uniform refinement of the control volume into 4 equal sub-cells by the horizontal and vertical bi-section lines (Figure 3). More sophisticate approaches include the identification of the refined directions for rectangular partitioning (Figure 4a), construction of non-uniform initial grids by the use of pre-priori estimation (Figure 4b), the lessening of sudden changes of grid sizes by adding smoothing nodes around the refined areas, (Figure 4c) and the use of other shapes, such as triangles, to facilitate complex geometries as well as to better capture the fluxes diagonally across the rectangles (Figure 4d).

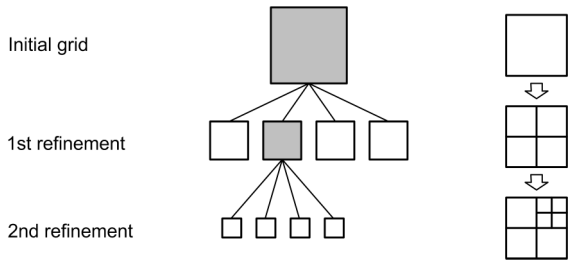

Figure 3 Uniform rectangular refinement [7]

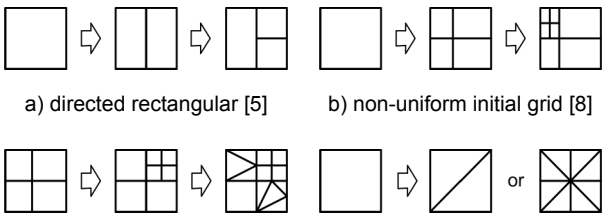

a) directed rectangular [5] b) non-uniform initial grid [8]

c) hybrid-shape grid [9] d) triangular refinement [10]

Figure 4 Other refinement techniques for initial rectangular grids

This paper proposes a new refinement criterion which is based upon the discrepancy of primary variables between the volume integration and face interpolation. First, the heat conduction is used as an example of PDEs. Then, the simulation of the governing equation by unstructured, cell-centred finite volume method is outlined, followed by the descriptions of the proposed residual error estimation and the refinement criterion. The control volumes are refined in the simplest manner: the uniform h - refinement of rectangular grids (Figure 3). Then, a 2D test case is used to preliminary verify the procedure.

2. Simulation by Finite Volume Method

The 2D mathematical model of heat conduction is formulated and discretised by a cell-centred finite volume technique for unstructured grids [3], [11]. The advantages of this scheme include the direct representation of conservative laws and straightforward physical interpretation.

2.1 Mathematical Models

The law of conservation of the energy in solid is employed as the governing equation. With the Fourier's law of heat conduction for isotropic materials, the mathematical model takes the form:

$$\frac{d}{dt}\int_V \rho c T \, dV = \int_{S_i} k \frac{\partial T}{\partial x_i} \, dS_i + \int_V Q \, dV \,, \tag{1}$$

where V is the volume of a body, bounded by the surface which is presented by the normal, outwards vector S_i, t is the time, ρ is the density, c is the specific heat, T is the temperature, k is the thermal conductivity, x_i is the position vector and Q is the heat source.

For bodies in thermal equilibrium without internal heat source, equation (1) is reduced to the diffusion term:

$$\int_{S_i} k \frac{\partial T}{\partial x_i} \, dS_i = 0 \,. \tag{2}$$

2.2 Spatial Discretisation

The spatial domain is discretised into a finite number of control volumes or cells. A typical cell (Figure 5), represented by the node P at the centre, is bounded by nb number of cell faces f with surfaces S_i^f, which. are shared between P and adjacent cells Q^f. In addition, non-computational nodes at boundaries are introduced for the specification of boundary conditions.

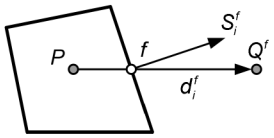

Figure 5 A typical unstructured control volume of which $nb = 4$

2.3 Approximation of Diffusion Flux

The equation (2) can be exactly expressed for any cell P as:

$$\int_{S_i} k \frac{\partial T}{\partial x_i} \, dS_i = \sum_{f=1}^{nb} \int_{S_i^f} k \frac{\partial T}{\partial x_i} \, dS_i^f = \sum_{f=1}^{nb} k (\frac{\partial T}{\partial x_i})^f S_i^f \,. \tag{3}$$

The method assumes the second-order accurate spatial distribution for any variable. That is, the truncation error ε is proportional to δx^2, where δx is the cell size. The value of any quantity ϕ at a cell face f between P and Q^f is calculated by:

$$\phi^f = \frac{\phi^P + \phi^{Q^f}}{2} + \frac{g_i^P (r_i^f - r_i^P) + g_i^{Q^f} (r_i^f - r_i^{Q^f})}{2} \,, \tag{4}$$

where g_i is the gradient of ϕ, r_i is the position vector and the superscript denotes the location of the property. The gradient vector g_i at cell P is calculated by ensuring a least square fit of ϕ through P and neighbouring nodes Q^f as:

$$(\sum_{f=1}^{nb} d_j^f d_i^f) g_i^P = \sum_{f=1}^{nb} (\phi^P - \phi^{Q^f}) d_j^f \,, \tag{5}$$

where $d_i^f = r_i^{Q^f} - r_i^P$ is the distance vector between P and Q^f.

Thus, the diffusion flux throught the cell face f into neighboring nodes Q^f can be approximated by the orthogonal correction approach as:

$$k(\frac{\partial T}{\partial x_i})^f S_i^f \approx k \frac{S^f}{d^f} (T^{Q^f} - T^P) + k(\frac{\partial T}{\partial x_i})^f (S_i^f - \frac{S^f}{d^f} d_i^f) \,. \tag{6}$$

2.4 Solution Algorithm

The equation (6) for each control volume may be rearranged into:

$$(\sum_{f=1}^{nb} k\frac{S^f}{d^f})T^P - \sum_{f=1}^{nb}(k\frac{S^f}{d^f}T^{Q^f}) = \sum_{f=1}^{nb}\left(k(\frac{\partial T}{\partial x_i})^f(S_i^f - \frac{S^f}{d^f}d_i^f)\right). \quad (7)$$

By assembling equation (8) of all *nc* control volumes in the domain, the system of simultaneous algebraic equations $[A]\cdot[T]=[b]$ is formed with nodal temperature $[T]$ as unknowns. The system is linearised, segregate and then iteratively 'solved' by the incomplete Cholesky conjugate gradient (ICCG) solver until a certain level of convergence is reach. The updated results are then used to recalculate the non-linear terms and the new system is again 'solved'. This procedure is repeated until implicit solutions are obtained.

3. Refinement Identification

The main contribution of this paper is the proposition of a general residual error estimator for the calculation of refinement parameter. As usual, the primary variable of the governing equation ϕ is used as the control parameter. Instead of using the double gradient $\nabla^2\phi$ as previously described, a simplified residual estimator, based on discrepancy between the volume integration and face interpolation [12], is presented.

3.1 Residual Error Estimation

As FVM formally integrates the mathematical model over each control volume, the surface integrals of governing equations is integrated with interpolations of the cell face values as shown in (4). Hence, the nodal values of ϕ depends on values of neighbouring control volumes through the common cell face values and the gradient of ϕ. This observation leads to an estimation of residual by the inconsistency between the volume integration and face interpolation [12].

Assuming the linear variation of dependent variable ϕ between a cell *P* and Q^f, the value at position A^f, located exactly half-way between *P* and Q^f, is calculated by linear interpolation between the two nodes as:

$$\phi^{A^f} = \frac{\phi^P + \phi^{Q^f}}{2}. \quad (8)$$

Alternatively, the value at point A^f can be obtained from the linear projection from cell *P* alone and the function (4) is shortened to:

$$\tilde{\phi}^{A^f} = \phi^P + g_i^P(r_i^{A^f} - r_i^P). \quad (9)$$

For better visualisation, the relationships maybe simplified to 1D as shown in Figure 6.

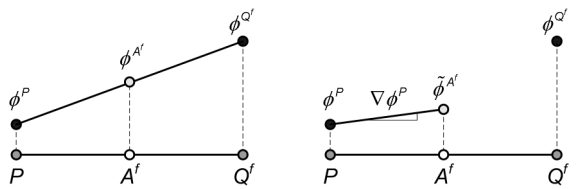

a) interpolation for ϕ^{A^f} b) projection from *P* for $\tilde{\phi}^{A^f}$

Figure 6 1D cell face interpolation

For an arbitrary point A^f between cells *P* and Q^f, the values of ϕ^{A^f} and $\tilde{\phi}^{A^f}$, respectively obtained from (8) and (9), are identical in case of linear variation of the solution over the control volume *P* and its neighbours, in which case the numerical error is zero.

Hence, the difference between the two methods is used to indicate the quality of variable profiles over the domain, resulting in a simplified version of residual estimator. Steep changes of solution gradients between adjacent nodes, relative to the overall outlook of the entire solutions, are sure indicators of errors and, thus, more nodes are required as, ideally, the residual error distributions in the domain should be close to zero.

3.2 Grid Refinement Indicator

For a given control volume *P*, the residual indicator is based on summation of solution inconsistency between (8) and (9) at various locations A^f around the cells, specifically the mid points between *P* and its adjacent nodes that share cell faces (Figure 7). The mean residual of control variable of a cell *P,* $\bar{\varepsilon}^P$, is calculated by.

$$\bar{\varepsilon}^P = \frac{1}{nb}\left(\sum_{f=1}^{nb}|\phi^{A^f} - \tilde{\phi}^{A^f}|\right). \quad (10)$$

The overall quality of the residual error in the domain is represented by the mean of residuals ε_M of all *nc* control volumes as:

$$\varepsilon_M = \frac{1}{nc}\left(\sum_{P=1}^{nc}|\bar{\varepsilon}^P|\right). \quad (11)$$

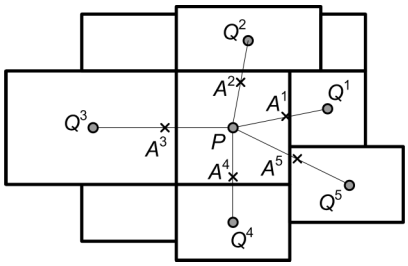

Figure 7 Residual calculation points around a typical cell *P*

In order to ensure that all nodal residual errors of the domain are relatively uniform, implying that there are no abrupt changes of variable gradient profile in the final solution set, the refinement indicator c_ε is taken to be the multiplication of a refinement factor f_{ε_M} with the mean residuals ε_M:

$$c_\varepsilon = f_{\varepsilon_M}\varepsilon_M. \quad (12)$$

The mean residual of all control volumes are compared with this refinement indicator c_ε and those with mean nodal residual error $\bar{\varepsilon}^P$ above c_ε are uniformly divided for the next grid level as shown in Figure 8.

The refinement factor f_{ε_M} influences the rate of grid independent convergence between grid levels; the lower values of f_{ε_M}, the higher numbers of cells are tagged for refining and vice versa. Hence, The values of refinement factor f_{ε_M} may be adjusted between different grid levels. The use of $f_{\varepsilon_M} < 1.0$ or $c_\varepsilon < \varepsilon_M$ may be appropriate for the initial levels of adaptive meshes. Then, the f_{ε_M} may be gradually increased with some

evidences of grid independency convergences, such as the lowering number of control volumes that are refined in different grid levels as the LGR procedure progresses. Nonetheless, the final value of f_{ε_M} must exceed 1.0 to ensure the termination of the LGR algorithm.

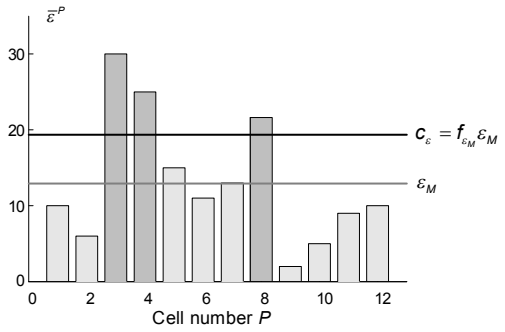

Figure 8 Cell refinement identification

4. Test Case

A 2D heat conduction test case with the domain of width w and height h (Figure 9a) is used to check the proposed LGR algorithm. For a material with constant conductivity k, the exact temperature solutions of this problem is obtained by the method of superposition [13] such that:

$$T_{ana}^{(x_1,x_2)} = \frac{200}{\pi}\sum_{n=1}^{\infty}\frac{(-1)^{n+1}+1}{n}\left[T_1(x_1,x_2)+T_1(x_1,x_2)\right],$$
$$T_1(x_1,x_2) = \sin(n\pi x_1/w)\frac{\sinh(n\pi x_2/w)}{\sinh(n\pi h/w)},$$
$$T_2(x_1,x_2) = \sin(n\pi x_2/h)\frac{\sinh(n\pi x_1/h)}{\sinh(n\pi w/h)}, \qquad (13)$$

with the resulting contours shown in Figure 9b.

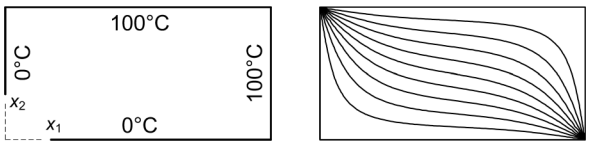

a) boundary condition b) analytical temperature

Figure 9 Descriptions and analytical solutions of the test case

Initially, the domain is divided into an 8-by-4 grid with the solutions and residuals used to determine the next level refinement in Figure 10a. The nodal error err^P and percentage errors $err_{\%}^P$ are defined as:

$$err^P = T^P - T_{ana}^P,\ err_{\%}^P = 100(T^P - T_{ana}^P)/T_{ana}^P, \qquad (14)$$

while the mean normalised $\overline{err_{\%}}$ and normalised standard deviation $SD_{err_{\%}}$ of $err_{\%}^P$ is normalised by the cell volumes to take into account the sizes of control volumes such that:

$$\overline{err_{\%}} = \left(\sum_{P=1}^{nc} err_{\%}^P\left|V^P\right|\right)\Big/\sum_{P=1}^{nc}V^P,$$
$$SD_{err_{\%}} = \left(\sum_{P=1}^{nc}(err_{\%}^P - \overline{err_{\%}})^2 V^P\Big/\sum_{P=1}^{nc}V^P\right)^{1/2}. \qquad (15)$$

The temperature is used as the control parameter ϕ of the refinement procedure or $\phi = T$ in equations (10) and (11). Because of the high errors in the initial mesh, the lower values of refinement factors f_{ε_M} are used in the first two levels to increase numbers of refined control volumes while the prescribe value for following levels are kept constant thereafter. That is, the refinement parameter c_ε for each grid level is obtained from the successive factorisation of ε_M by $f_{\varepsilon_M} = 0.75$ for first adaptive level, 0.90 for the second, and 1.10 for all others.

After the initial results, the grids are locally refined and solved as previously described with series of meshes and residuals in Figure 10 and key values summarised in Table 1. Additionally, the nodal residuals and the refinement indicators are shown in Figure 11. Normally, the LGR procedure is terminated when there is no more control volume that satisfies the refinement criterion of $\bar{\varepsilon}^P > c_\varepsilon$.

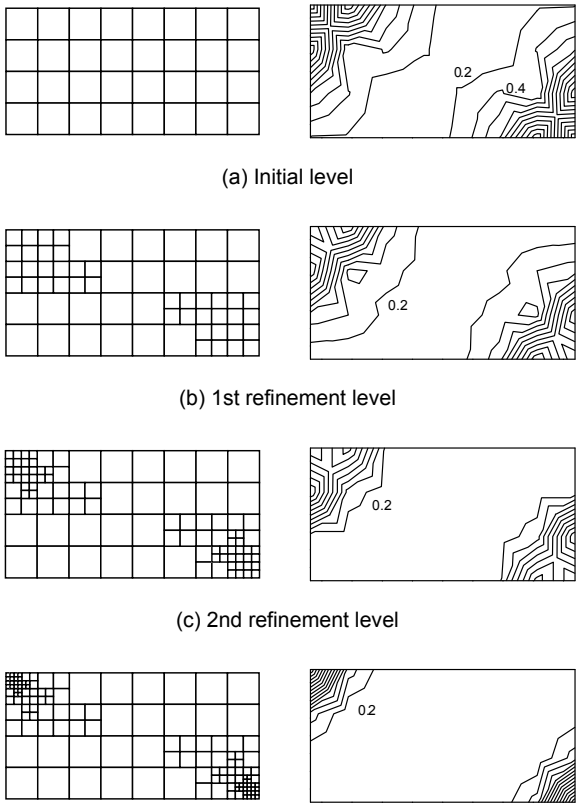

(a) Initial level

(b) 1st refinement level

(c) 2nd refinement level

(d) 3rd refinement (final) level

Figure 10 Mesh refinement of test cases: grids (left), residuals $\bar{\varepsilon}^P$ (right, contour level = 0.2°C)

In the refinement algorithm, larger numbers of cells in critical areas help obtaining the numerical results that approaches the exact solutions. Finally almost all the individual cell errors reduce to an acceptable level with relatively flat nodal gradient of solutions (Figure 11). There are, however, two groups of control volumes with particularly high residuals at opposite corners of the domain. This is due to the singularity of the corner boundary conditions where the prescribed temperatures are different at the adjoining edges. Thus, cells in these two areas can be refined practically indefinitely. When the temperature errors are considered, the maximum errors that hardly decrease across the refinement levels is caused by theses singularity points as well.

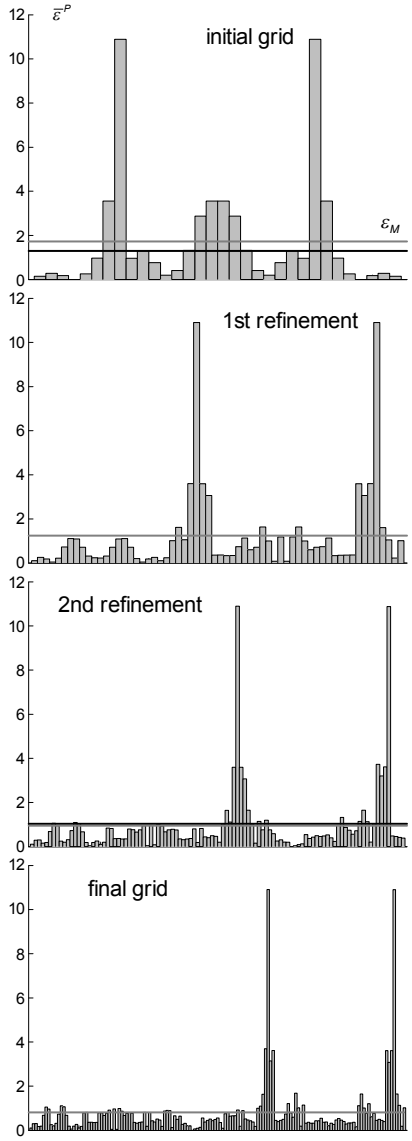

Figure 11 Nodal values of residual errors

Table 1 Refinement overview of the test case

mesh refinement	initial	1st	2nd	final
no. of cells	32	62	98	134
no. of cells to be refined	10	12	12	-
area to be refined, % domain	31.25	9.375	2.343	-
maximum $\lvert err^P \rvert$, °C	2.189	2.200	2.122	2.284
maximum $err^P_{\%}$, %	12.07	10.88	10.60	10.90
$\overline{err_{\%}}$, %	0.487	0.258	0.177	0.173
$SD_{err_{\%}}$, %	3.498	2.392	2.029	1.41
maximum $\bar{\varepsilon}^P$, °C	10.89	10.89	10.90	10.90
SD of $\bar{\varepsilon}^P$, °C	2.67	2.007	1.633	1.41
residual error indicator ε_M, °C	1.73	1.245	0.998	0.802
refinement factor f_{ε_M}, %	75	90	110	-

It is, thus, shown that after the final refinement, in which control volumes outside singularity zones are no longer tagged for refinement, the solution converges to steady values. This condition is called grid independency and further refinement will not affect the solution.

5 Discussions and Conclusions

A preliminary study on the LGR by a simplified residual error estimator is presented. The grid independent solutions of 2D heat conduction problems are obtained by finite volume simulation with the localised *h*-refinement. The domain is first divided into a coarse grid from which the numerical solutions are obtained. The problematic regions in the domains, identified by the residual errors and prescribed refinement factors, are refined until all nodal residuals are suitably lowered to a fairly even level.

As this paper presents \preliminary studies of the proposed LGR, future works are divided into the development and extension sections. The development works includes 1) further verifications with more difficult problems and comparisons with other established LGR, 2) the utilisation of other LGR techniques described in the introduction as appropriate, 3) the study on the refinement factor f_{ε_M}, both on its effects on the rate of convergence and the generalised suitable values, with automatic adjustments, and 4) the utilisation of cell combining in areas with low residual errors in addition to the current refinements. The extension works involve 1) the uses of other cell shapes, i.e. triangles and general tetragons, to take advantages of unstructured grid discretisation for complex geometries, 2) uses of LGR in other mathematical models, starting with thermal stress analyses, as well as 3) applications to real problems, specifically to automatically obtain grid independent solutions for evolutionary continuum topology designs [14].

6 Acknowledgement

This work is partially supported by TRF for the Senior Research Scholar Prof. Pramote Dechaumphai.

References

[1] G. Edwards, “Elimination of adaptive grid interface errors in the discrete cell-centered pressure equation”, Journal of Computational Physics, 1996, vol. 126, pp. 356-372

[2] V. Juntasaro and V. Pongboonchu, “Evaluation of multilevel fast adaptive composite grid method for transient heat transfer problem”, Proceedings of ME-NETT16, 2002, TF 114, pp. 55-59

[3] S. Muzaferija, “Adaptive Finite Volume Method for Flow Predictions Using Unstructured Meshes and Multigrid Approach”, 1994, PhD Thesis, Imperial College

[4] R. L. Verweij, R. Twerda and T. W. J. Peeters, “Parallel computing for reacting flows using adaptive grid refinement”, Contemporary Mathemaics, 1998, vol. 218, pp. 538-546

[5] F. E. Ham, F. S. Lien and A. B. Strong, “A Cartesian grid method with transient anisotropic adaptation”, Journal of Computational Physics, 2002, vol. 179, pp. 469-494

[6] P. A. Durbin and G. Iaccarino, “An approach to local refinement of structured grids”, Journal of Computational Physics, 2002, vol. 181, no. 2, pp. 639-653

[7] C. W. Lan, C. C. Liu and C. M. Hsu, “An adaptive finite volume method for incompressible heat flow problems in solidification”, Journal of Computational Physics, 2001, vol. 178, no. 2, pp. 464-497

[8] B. A. V. Bennett and M. D. Smooke, “Local rectangular refinement with application to nonreacting and reacting fluid flow problems”, Journal of Computational Physics, 1999, vol. 151, pp. 684-727

[9] N. Provatas, N. Goldenfeld and J. Dantzig, “Adaptive mesh refinement computation of solidification microstructures using dynamic data structures”, Journal of Computational Physics, 1998, vol. 148, no. 1, pp. 265-290

[10] D. Kim and H. Choi, “ A second-order time-accurate finite volume method for unsteady incompressible flow on hybrid unstructured grids”, Journal of Computational Physics, 1999, vol. 162, pp. 411-428

[11] K. Maneeratana and A. Ivankovic, “Finite volume method for structural applications involving material and geometrical non-linearities”, Proceedings of ECCM’99, Germany, 1999, no. 325

[12] H. Jasak, and A.D. Gosman, “Element residual error estimate for the finite volume method”, Computer & Fluids, 2003, vol. 32, pp.223-248

[13] J. P. Holman, “Heat Transfer”, McGraw Hill, 2001

[14] K. Boonlong and K. Maneeratana. “A preliminary study on the multi-objective topology design by genetic algorithm and finite volume method”, Proceedings of ME-NETT17, 2003, CS024.